

ChemComm

Accepted Manuscript



This is an *Accepted Manuscript*, which has been through the Royal Society of Chemistry peer review process and has been accepted for publication.

Accepted Manuscripts are published online shortly after acceptance, before technical editing, formatting and proof reading. Using this free service, authors can make their results available to the community, in citable form, before we publish the edited article. We will replace this *Accepted Manuscript* with the edited and formatted *Advance Article* as soon as it is available.

You can find more information about *Accepted Manuscripts* in the [Information for Authors](#).

Please note that technical editing may introduce minor changes to the text and/or graphics, which may alter content. The journal's standard [Terms & Conditions](#) and the [Ethical guidelines](#) still apply. In no event shall the Royal Society of Chemistry be held responsible for any errors or omissions in this *Accepted Manuscript* or any consequences arising from the use of any information it contains.



Journal Name

COMMUNICATION

Three-dimensional Hierarchical Prussian blue Composed of Ultrathin Nanosheets: Enhanced hetero-catalytic and adsorption properties

Received 00th January 20xx,
Accepted 00th January 20xx

DOI: 10.1039/x0xx00000x

Fan-Xing Bu, Ming Hu, Wei Zhang, Qi Meng, Li Xu, Dong-Mei Jiang and Ji-Sen Jiang*

www.rsc.org/

Three-dimensional hierarchical Prussian blue composed of ultrathin nanosheets were successfully synthesized by employing self-aggregation and oriented attachment strategy. The unique structure highly increases the exposure of micropores and metal sites of Prussian blue to guests, thus significantly enhances its hetero-catalysis and adsorption properties compared to cubic and commercial counterparts.

Coordination polymers (CPs), including porous coordination polymers (PCPs) or metal-organic frameworks (MOFs), have attracted extensive attention because their adjustable functional components (including metal ions, organic linkers and pores) could be used as functional sites for various applications, such as pores for molecules (or ions) adsorption and separation, and metal active sites for catalysis.¹ To obtain CPs with optimized properties, we have to maximize or optimize the use of these functional components by making them accessible to exotic guests in an effective and even efficient way. Two promising strategies could be adopted to realize this goal. The first one is the creative construction of new CPs with larger pores or higher surface area by adjusting their components and crystal structures,² and the second one is effective design of structured CPs with more external surface and shorter diffusion length by their morphology and size control.³ The former is so convenient that most of previous efforts have been devoted to this respect, and large amount of CPs has been achieved. While, the latter has just begun to attract growing attentions in recent years because the structured CPs showed outstanding and impressive performance compared to bulk CPs. For example, engineering Prussian blue (PB) and Prussian blue analogues (PBAs) into complex hollow structure significantly increases gas and ion adsorption properties.^{3b,3c} Tailoring $\text{Cu}_3(\text{BTC})_2$ into mesoporous structure could largely enhance the catalytic property for aerobic oxidation of benzylic alcohols.^{3d} These intriguing and pioneered

results open the door for the structural modification of CPs, which needs more research.

Among various structures, two-dimensional (2D) CPs with ultrathin thickness (several nanometers) have achieved considerable attention, for they could expose large amount of functional components to the exterior surface of CPs and make these functional components easily accessible to guests.⁴ This makes 2D CPs with ultrathin thickness the ideal candidates that can adequately use the functional components of CPs. For instance, MOF nanosheets have presented ultra-permeability and high selectivity when used as building blocks for molecular sieving membranes.^{4d,4e} However, owing to their high surface energy and interlayer van der Waals attractions, 2D nanostructures tend to re-stack and condense during practical applications, which greatly decrease the performances in many applications. Referring to previous reports on hierarchical inorganic materials, organizing them into three-dimensional (3D) hierarchical architectures would be one wonderful route to resolve this problem.⁵ Moreover, the three-dimensionalization of two-dimensional nanosheets may provide extra mesopores and even macropores, which would promote more effective transport of guest molecules and ions⁶ and endow these materials promising applications in environment and energy fields.

Recently, several efforts have been made towards the preparation of hierarchical CPs composed of nanosheets (HCPN).⁷ Kitagawa et al. designed 3D HCPN by pseudomorphic replication method.^{7a} Yaghi et al. fabricated ordered and oriented HCPN on plasmonic silver nanocrystals.^{7b} We also developed one versatile strategy to construct multifunctional metal oxide@cyanometallate-based coordination polymer heterostructures and hierarchical shell constructed by PBA nanosheets can be successfully grown on the surface of the metal oxide.^{7c} However, these strategies are relatively complex, which need additional exotic substrates for the confined growth of CPs nanosheets. In addition, all these reported CPs nanosheets are of 2D layered crystal structure and no CPs nanosheets with highly symmetric crystal structure have been reported. Thus the fabrication of HCPN still faces enormous challenges and it is wonderful to develop new and simple one-pot synthetic methods for further extensive research of HCPN with

Department of Physics, Center for Functional Nanomaterials and Devices, East China Normal University, Shanghai 200241, P.R. China.

E-mail: jsjiang@phy.ecnu.edu.cn

† Electronic Supplementary Information (ESI) available: [more details of synthesis and characterizations including XRD, FT-IR, Mössbauer spectrum, SEM and TEM]. See DOI: 10.1039/x0xx00000x

highly symmetric crystal structure. It has been demonstrated that non-classical crystallization with following treatment⁸ is one versatile way to construct hierarchical CPs and oriented attachment⁹ is one powerful route to synthesize nanosheets with highly symmetric crystal structure. As a proof of concept, we employed the nonclassical crystallization and external oriented attachment strategy to fabricate hierarchical PB composed by ultrathin nanosheets (HPBN). Here, PB with highly symmetric face-centred-cubic (FCC) crystal structure was elected as the model material, because PB and PBAs with face-centred-cubic (FCC) crystal structure have been always receiving considerable research interest due to their potential applications in molecular magnets, biomedical materials, catalysis, ion adsorption and cathode materials of secondary batteries.^{3c, 8a, 10} As except, the HPBN possess large amounts of exposed metal reactive sites and micropores, and exhibits superior catalytic degradation of MB and adsorption of Cs⁺ compared to their cubic and commercial counterparts. This demonstrates that constructing 3D hierarchical structure composed by 2D ultrathin nanosheets is one effective way to highly enhance the use of functional components of coordination polymers and improve their properties.

The HPBN were prepared by solvothermal treatment of potassium ferricyanide and hydrochloric acid in the mixture of water/ N,N-dimethylformamide (DMF) (please see the details in ESI[†]). X-ray diffraction (XRD) profile (Fig. S1) demonstrates that the obtained products are pure phase PB with face-centred-cubic lattice (JCPDS 73-0687).¹¹ Fourier transform infrared spectroscopy (FTIR) (Fig. S2) and Mössbauer spectroscopy (Fig. S3) were used to further confirm the composition of the products. The strong absorption peaks at 2084 cm⁻¹ is characteristic CN stretching absorption bands of PB.¹¹ The absorption band at around 602 cm⁻¹ and 498 cm⁻¹ are due to the structure of Fe^{II}-CN-Fe^{III} linkage. The Mössbauer spectrum of the product contains a singlet absorption peak (the isomer shift is -0.15 mm/s) and a doublet absorption peak (the isomer shift is 0.33 mm/s and the quadrupole splitting is 0.47 mm/s), which are attributed to the low spin Fe^{II} and the high spin Fe^{III}, respectively.

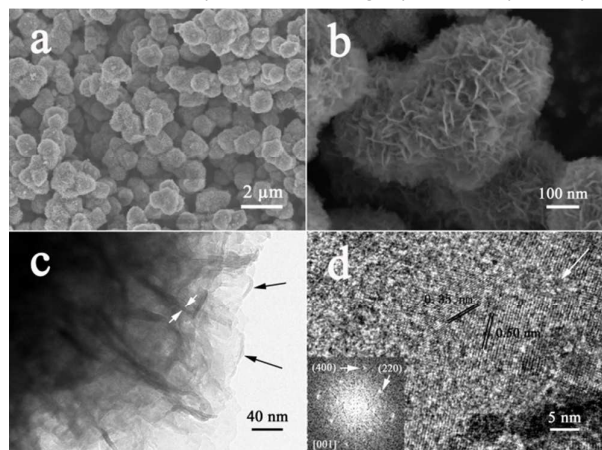


Fig. 1 (a) and (b) FESEM images of sample prepared following a typical procedure. (c) TEM image of the edge of a HPBN and (d) High magnification TEM image of the edge of a nanosheet. (Inset: Corresponding FFT image indexed to the [001] zone)

The morphology and hierarchical structure of the typical HPBN are presented in Figure 1. FESEM measurements show that the

obtained samples are hierarchical PB with their size ranging from 500 nm to 1.5 μm (Fig. 1a). The hierarchical structure was constructed by numerous interconnected ultrathin nanosheets (Fig. 1b). This observation is further confirmed by TEM examination in Fig. 1c. It is to be noted that these nanosheets are all almost wrinkled and the edge of certain sheets crimped as indicated by inset black arrows, demonstrating these nanosheets has a certain of flexibility. The thickness of the nanosheet is estimated to be around 5 nm (as indicated by inset white arrows) from the nanosheets that are oriented approximately perpendicular to the supporting film. The crystal facets of the nanosheet subunits were determined by high-resolution TEM (HRTEM) and the visible lattice fringes were observed on edge of a single nanosheet (Fig. 1d). The observed lattice distances of 0.5 nm and 0.35 nm correspond to the inter-plane spacing of (200) and (220) of face-centred-cubic PB (JCPDS card no. 73-0687), respectively. The fast Fourier transform (FFT) pattern of the same region (Fig. 1d, inset) can be indexed to diffraction spots of the [001] zone, which corresponds to the surface exposure of (001) facets of PB. It is to be noted that there existed many defects in the nanosheets as indicated by white arrow. This would provide extra pores and much more active sites for their application in hetero-catalysis and adsorption.

To shed light on the formation mechanism of the HPBN, time-dependent experiments were conducted. FESEM pictures of the products collected at different reaction stages were shown in Fig. S4. Firstly, nanoparticles were formed at 1.5 h (Fig. S4a) and then aggregated into irregular particles with rough surface at 2 h (Fig. S4b). When the reaction proceeded to 3 h, honeycomb-like particles with their surface covered by large amounts of nanosheet-like protuberances appeared (Fig. S4c). From the high magnification SEM picture of the edge of one single particle (Fig. S4d), it can be observed that these nanosheets do not existed independently and demonstrate randomly interconnected structure. Surprisingly, high magnification TEM picture in Fig. S4e displays that these nanosheets are ill-crystallized or amorphous. Along the reaction proceeded (9 h), products with their surface covered by well-defined nanosheets were produced (Fig. S4f and S4g). As shown in Fig. S4h, crystallized nanoparticles enclosed by ellipses formed among the amorphous matrix in the nanosheets. With further reaction, these nanosheets would crystallize and well-defined HPBN were obtained.

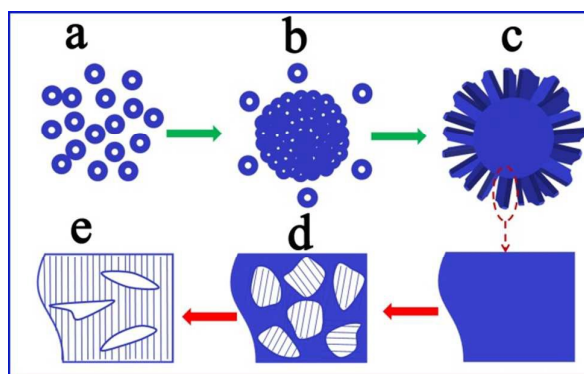


Fig. 2 Schematic illustration of the formation process of HPBN. (Green arrows donate self-aggregation process and red arrows refer to oriented attachment process.)

Based on the above analysis, the mechanistic formation mechanism of HPBN based on self-aggregation and oriented attachment was proposed as shown in Figure. 2. At first, large amounts of nanoparticles were formed rapidly due to high supersaturation degree at the initial stage (Fig. 2a). Then these nanoparticles self-assembled into irregular particle aggregations owing to the high surface energy (Fig. 2b).^{8a, 12} At the following reaction process, reaction kinetic was largely slowed by the depletion of reactants. By using the previously formed particle aggregations as nucleation sites, amorphous nanosheets were formed by further self-aggregation of PB nanoparticles (Fig. 2c). Then PB nanoparticles crystallized in these nanosheets (Fig. 2d) and then oriented attachment took place to decrease the system energy (Fig. 2e).¹³ At last, HPBN composed by well-crystallized PB nanosheets formed.

It is well-known that PB nanoparticles with cubic morphology were always the building blocks of PB obtained by common non-classical crystallization processes.^{8b,8c} Obviously, the formation process of HPBN is another kind of non-classical crystallization process that different from the previous reports. So, it is highly important to reveal the crucial factors that dominated this non-classical crystallization process. The species and content of solvent were disclosed as the most important factors. When DMF was changed into dimethylacetamide, ethanol and formamide, it was found that only reaction system using dimethylacetamide produced HPBN (Fig. S5). While, cubic PB were prepared by employing ethanol (Fig. S6) and formamide (Fig. S7). In addition, increasing the volume ratio of water/DMF from 5/25 to 10/20 and 15/15 lead to irregular cubic aggregations (Fig S8). However, the concrete driving force for the formation of PB nanosheets needs further research. In spite of this, this reaction system is versatile and could be used to synthesize HPBN by changing potassium ferricyanide into sodium ferrocyanide and potassium ferrocyanide (Fig S9). And the synthesis of PBAs with face-centred-cubic structure is ongoing and will be presented on our further works.

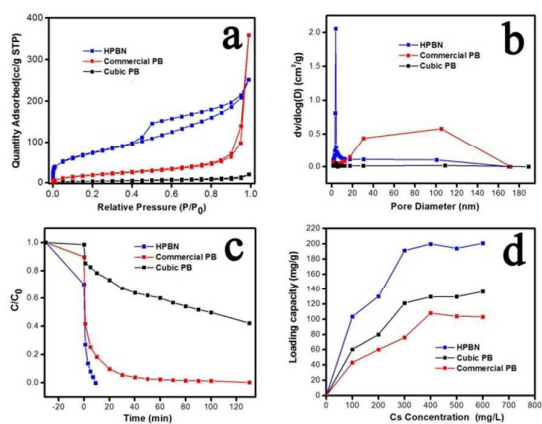


Fig. 3 (a) N_2 adsorption-desorption isotherms and (b) Corresponding BJH mesopore-size distribution curves, (c) The time-dependent degradation curves of MB and (d) Adsorption isotherms of Cs^+ of HPBN, cubic PB and commercial PB.

Nitrogen sorption analysis was performed to investigate the specific surface area and porosity of such 3D hierarchical structures. Cubic PB microcrystals (Fig. S8c and S8d) and irregular commercial PB nanoparticles (Fig. S10) were used as comparisons. For HPBN, a

drastic increase in the N_2 adsorption-desorption isotherm (Fig.3a) at low relative pressure ($P/P_0 < 0.01$) was observed, indicating the presence of inherent micropores of the HPBN. However, only low N_2 uptake in the same range was observed for cubic PB and commercial PB (Fig.3a). Generally, it is difficult for N_2 to enter into the interior of PB.^{3b,3c} Therefore, these results may indicate more exposed surface of HPBN than cubic PB and commercial PB. The isotherms of HPBN (Fig.3a) also presented a hysteresis loop in the range of $P/P_0 = 0.4-1.0$, meaning that the HPBN particles contained constricted mesopores that were formed by organization of nanosheets. This was confirmed by corresponding concentrated mesopore size distribution on 3.8 nm (Fig 3b) obtained from BJH analysis. But wide pore distributions caused by random packing of particles were observed in cubic PB and commercial PB (Fig 3b). The hierarchical structure makes HPBN have a highest Brunauer-Emmett-Teller (BET) surface area among these three samples ($246 \text{ m}^2 \text{ g}^{-1}$ for HPBN, $73 \text{ m}^2 \text{ g}^{-1}$ for commercial PB, $15 \text{ m}^2 \text{ g}^{-1}$ for cubic PB). The N_2 sorption results completely confirm the advantage of 3D hierarchical structure composed by ultrathin nanosheets, indicating that the HPBN maybe a good candidate in applications such as hetero-catalysis and adsorption.

Motivated by the hierarchical structure and ultrathin nanosheets subunits of the HPBN, we firstly examined the Fenton-like catalysis property of HPBN on the degradation of methylene blue (MB). MB was selected as a model target because it is one of the most commonly used dyes in various industries and had been widely used as probe compound for the advanced oxidation process.^{8a} According to the time-dependent degradation curves of MB in Fig. 3c, it can be found that 73% of MB had been removed within 1 min in the presence of HPBN while only 25% for cubic PB and 55% for commercial PB. Moreover, all MB was degraded by HPBN at 9 min while 130 min and 24 h are needed for commercial and cubic PB to remove all MB. This should be mainly originated from two points. Firstly, the HPBN provide higher BET surface area than commercial PB and cubic PB, and thus more Fe^{II} reactive sites, this could be further demonstrated by different adsorption content of MB before the degradation (30%, 10% and 2% for HPBN, commercial PB and cubic PB, respectively). Secondly, the hierarchical structure could effectively prevent the loss of Fe^{II} reactive sites caused by agglomeration of particles and large amount of mesopores in the hierarchical structure could more effectively promote the transport of MB and degradation products.

At the same time, their adsorption property of radioactive ions was also evaluated. Cs^+ was chosen as the typical toxic ions because the isotope ^{137}Cs is the most critical radionuclide in power plant waste and it has been reported that PB exhibits strong affinity for Cs ions.^{3c, 10f, 10g} As shown in Fig. 3d, the saturated adsorption capacity of HPBN is about 200 mg/g, which is higher than that of (about 135 mg/g) cubic PB and (about 105 mg/g) commercial PB. Herein, through HPBN with highest BET surface area exhibited the best Cs^+ adsorption property, cubic PB with the lowest BET surface area manifested better performance than commercial PB with medium BET surface area. It is well-known that the exterior micropores^{10f} and internal vacancies^{10g} of PB could all accommodate Cs^+ , it is possible that cubic PB have more vacancies in their interior. This was confirmed by ICP analysis on all three samples. It was found that atom ratio of K:Fe in HPBN, cubic PB and commercial PB is

12.2:100, 1.48:100 and 6.93:100, respectively. Generally, less K^+ ions mean more vacancies in the internal PB lattice and thus more Cs^+ could be accommodate in the internal of PB lattice.^{10h} Thus cubic PB with lowest BET surface area showed medium adsorption capacity owing to its most vacancies. The above results demonstrate that increasing exposed micropores and crystal lattice vacancy of PB are both effective routes to improve adsorption capacity of Cs^+ on PB. However, HPBN with the least vacancies still displayed the highest adsorption capacity, which further demonstrated the advantage of structuring coordination polymers into 3D structure composed by ultrathin nanosheets.

In summary, HPBN were prepared by one-pot solvothermal method. Self-aggregation and oriented attachment were revealed as the formation mechanism of the HPBN. The HPBN manifest a three-dimensional hierarchical structure with a high specific surface area of $256 \text{ m}^2 \text{ g}^{-1}$. Inspired by the highly enhanced exposure of metal active sites and micropores on the ultrathin PB nanosheets, we evaluated their catalysis and adsorption properties. This HPBN show remarkable catalysis performance in degradation of MB, about 13 and 140 times faster than commercial PB and cubic PB, and adsorption property of Cs^+ , about 1.5 and 2 times more than cubic PB and commercial PB. In addition, we anticipate that this HPBN may demonstrate interesting optical and magnetic properties and also show exciting performance in rechargeable batteries and sensors. Such results may open a promising method to prepare 3D hierarchical coordination polymers with highly symmetric crystal structures composed of ultrathin nanosheets, provide superior catalysts and adsorbent materials and offer a promising way to enhance the use of functional components of CPs.

Notes and references

This work was supported by the National Natural Science Foundation of China (Grant Nos. 21473059, 21173084, 21401056) and Large Instruments Open Foundation of East China Normal University.

- (a) J. Lee, O. K. Farha, J. Roberts, K. A. Scheidt, S. T. Nguyen and J. T. Hupp, *Chem. Soc. Rev.*, 2009, **38**, 1450; (b) N. Stock and S. Biswas, *Chem. Rev.*, 2011, **112**, 933; (c) S. Kitagawa, R. Kitaura and S. i. Noro, *Angew. Chem. Int. Ed.*, 2004, **43**, 2334; (d) A. C. McKinlay, R. E. Morris, P. Horcajada, G. Férey, R. Gref, P. Couvreur and C. Serre, *Angew. Chem. Int. Ed.*, 2010, **49**, 6260.
- (a) X.-S. Wang, S. Ma, D. Sun, S. Parkin and H.-C. Zhou, *J. Am. Chem. Soc.*, 2006, **128**, 16474; (b) K. Wang, D. Feng, T.-F. Liu, J. Su, S. Yuan, Y.-P. Chen, M. Bosch, X. Zou and H.-C. Zhou, *J. Am. Chem. Soc.*, 2014, **136**, 13983; (c) H. Furukawa, N. Ko, Y. B. Go, N. Aratani, S. B. Choi, E. Choi, A. Ö. Yazaydin, R. Q. Snurr, M. O'Keeffe, J. Kim and O. M. Yaghi, *Science*, 2010, **329**, 424.
- (a) S. Furukawa, J. Reboul, S. Diring, K. Sumida and S. Kitagawa, *Chem. Soc. Rev.*, 2014, **43**, 5700; (b) M. Hu, A. A. Belik, M. Imura and Y. Yamauchi, *J. Am. Chem. Soc.*, 2012, **135**, 384; (c) N. L. Torad, M. Hu, M. Imura, M. Naito and Y. Yamauchi, *J. Mater. Chem.*, 2012, **22**, 18261; (d) L. Peng, J. Zhang, Z. Xue, B. Han, X. Sang, C. Liu and G. Yang, *Nat Commun*, 2014, **5**, 4465.
- (a) P.-Z. Li, Y. Maeda and Q. Xu, *Chem. Commun.*, 2011, **47**, 8436; (b) M. Hu, S. Ishihara and Y. Yamauchi, *Angew. Chem. Int. Ed.*, 2013, **52**, 1235; (c) Y. Sakata, S. Furukawa, M. Kondo, K. Hirai, N. Horike, Y. Takashima, H. Uehara, N. Louvain, M. Meilikhov, T. Tsuruoka, S. Isoda, W. Kosaka, O. Sakata and S. Kitagawa, *Science*, 2013, **339**, 193; (d) Y. Peng, Y. Li, Y. Ban, H. Jin, W. Jiao, X. Liu and W. Yang, *Science*, 2014, **346**, 1356; (e) T. Rodenas, I. Luz, G. Prieto, B. Seoane, H. Miro, A. Corma, F. Kapteijn, F. X. Llabrés i Xamena and J. Gascon, *Nat Mater*, 2015, **14**, 48; (f) S. Motoyama, R. Makiura, O. Sakata and H. Kitagawa, *J. Am. Chem. Soc.*, 2011, **133**, 5640.
- (a) C.-Y. Jin, M. Hu, X.-L. Cheng, F.-X. Bu, L. Xu, Q.-H. Zhang and J.-S. Jiang, *Chem. Commun.*, 2015, **51**, 206; (b) M. Gao, W. Sheng, Z. Zhuang, Q. Fang, S. Gu, J. Jiang and Y. Yan, *J. Am. Chem. Soc.*, 2014, **136**, 7077.
- (a) J. Liu, T. Yang, D.-W. Wang, G. Q. Lu, D. Zhao and S. Z. Qiao, *Nat Commun*, 2013, **4**, 2798; (b) J. Tang, J. Liu, C. Li, Y. Li, M. O. Tade, S. Dai and Y. Yamauchi, *Angew. Chem. Int. Ed.*, 2015, **54**, 588; (c) T. Yang, R. Zhou, D.-W. Wang, S. P. Jiang, Y. Yamauchi, S. Z. Qiao, M. J. Monteiro and J. Liu, *Chem. Commun.*, 2015, **51**, 2518.
- (a) J. Reboul, S. Furukawa, N. Horike, M. Tsotsalas, K. Hirai, H. Uehara, M. Kondo, N. Louvain, O. Sakata and S. Kitagawa, *Nature Mater.*, 2012, **11**, 717; (b) Y. Zhao, N. Kornienko, Z. Liu, C. Zhu, S. Asahina, T.-R. Kuo, W. Bao, C. Xie, A. Hexemer, O. Terasaki, P. Yang and O. M. Yaghi, *J. Am. Chem. Soc.*, 2015, **137**, 2199; (c) F.-X. Bu, L. Xu, W. Zhang, C.-Y. Jin, R.-J. Qi, R. Huang and J.-S. Jiang, *Chem. Commun.*, 2015, **51**, 6198.
- (a) F.-X. Bu, M. Hu, L. Xu, Q. Meng, G.-Y. Mao, D.-M. Jiang and J.-S. Jiang, *Chem. Commun.*, 2014, **50**, 8543; (b) M. Hu, J. S. Jiang, R. P. Ji and Y. Zeng, *CrystEngComm*, 2009, **11**, 2257; (c) X.-J. Zheng, Q. Kuang, T. Xu, Z.-Y. Jiang, S.-H. Zhang, Z.-X. Xie, R.-B. Huang and L.-S. Zheng, *J. Phys. Chem. C.*, 2007, **111**, 4499.
- (a) C. Schliehe, B. H. Juarez, M. Pelletier, S. Jander, D. Greshnykh, M. Nagel, A. Meyer, S. Foerster, A. Kornowski, C. Klinke and H. Weller, *Science*, 2010, **329**, 550; (b) K.-S. Cho, D. V. Talapin, W. Gaschler and C. B. Murray, *J. Am. Chem. Soc.*, 2005, **127**, 7140.
- (a) C. R. Gros, M. K. Peprah, B. D. Hosterman, T. V. Brinzari, P. A. Quintero, M. Sendova, M. W. Meisel and D. R. Talham, *J. Am. Chem. Soc.*, 2014, **136**, 9846; (b) D. M. Pajerowski, M. J. Andrus, J. E. Gardner, E. S. Knowles, M. W. Meisel and D. R. Talham, *J. Am. Chem. Soc.*, 2010, **132**, 4058; (c) D. Asakura, C. H. Li, Y. Mizuno, M. Okubo, H. Zhou and D. R. Talham, *J. Am. Chem. Soc.*, 2013, **135**, 2793; (d) M. S. Kandanapitiye, B. Valley, L. D. Yang, A. M. Fry, P. M. Woodward and S. D. Huang, *Inorg. Chem.*, 2013, **52**, 2790; (e) M. Shokouhimehr, E. S. Soehnlén, J. Hao, M. Griswold, C. Flask, X. Fan, J. P. Basilion, S. Basu and S. D. Huang, *J. Mater. Chem.*, 2010, **20**, 5251; (f) T. Ceranic, D. Trifunovic, R. Adamovic, *Z. Naturforsch. B*, 1978, **33**, 1099. (g) M. Ishizaki, S. Akiba, A. Ohtani, Y. Hoshi, K. Ono, M. Matsuba, T. Togashi, K. Kanazizuka, M. Sakamoto, A. Takahashi, T. Kawamoto, H. Tanaka, M. Watanabe, M. Arisaka, T. Nankawa and M. Kurihara, *Dalton Trans*, 2013, **42**, 16049; (h) W.-J. Li, S.-L. Chou, J.-Z. Wang, Y.-M. Kang, J.-L. Wang, Y. Liu, Q.-F. Gu, H.-K. Liu and S.-X. Dou, *Chem. Mater.*, 2015, **27**, 1997. (i) S. Vaucher, M. Li and S. Mann, *Angew. Chem. Int. Ed.*, 2000, **39**, 1793. (j) T. Uemura and S. Kitagawa, *J. Am. Chem. Soc.*, 2003, **125**, 7814.
- F. X. Bu, C. J. Du, Q. H. Zhang and J. S. Jiang, *CrystEngComm*, 2014, **16**, 3113.
- (a) R. Q. Song and H. Cölfen, *Adv. Mater.*, 2010, **22**, 1301; (b) A. W. Xu, M. Antonietti, H. Cölfen and Y. P. Fang, *Adv. Funct. Mater.*, 2006, **16**, 903.
- (a) J. Ye, W. Liu, J. Cai, S. Chen, X. Zhao, H. Zhou and L. Qi, *J. Am. Chem. Soc.*, 2010, **133**, 933; (b) M. Niederberger and H. Cölfen, *Phys. Chem. Phys.*, 2006, **8**, 3271; (c) L. Xu, F.-X. Bu, M. Hu, C.-Y. Jin, D.-M. Jiang, Z.-J. Zhao, Q.-H. Zhang and J.-S. Jiang, *Chem. Commun.*, 2014, **50**, 13849.